catalysts

MDPI

Article

Newly Designed Ternary Metallic PtPdBi Hollow Catalyst with High Performance for Methanol and Ethanol Oxidation

Zhiping Xiong, Shumin Li, Hui Xu, Ke Zhang, Bo Yan and Yukou Du *

College of Chemistry, Chemical Engineering and Materials Science, Soochow University, Suzhou 215123, China; xeuiaxiong@163.com (Z.X.); lishumin329@126.com (S.L.); xuhui199303@163.com (H.X.); zhangke910222@163.com (K.Z.); boyan623@outlook.com (B.Y.)

* Correspondence: duyk@suda.edu.cn; Tel./Fax: +86-512-65880089

Academic Editor: Luísa Margarida Martins

Received: 13 June 2017; Accepted: 6 July 2017; Published: 10 July 2017

Abstract: This paper reported the fabrication of ternary metallic PtPdBi hollow nanocatalyst through a facile, one-pot, wet-chemical method by adopting sodium borohydride and polyvinylpyrrolidone as reducing agent and surfactant directing agent, respectively. The hollow structure offers novel morphology and large surface areas, which are conducive to enhancing the electrocatalytic activity. The electrocatalytic properties of hollow PtPdBi nanocatalyst were investigated systematically in alkaline media through cyclic voltammetry and the as-prepared PtPdBi nanocatalyst displays greatly enhanced electrocatalytic activities towards methanol and ethanol oxidation. The calculated mass activities of PtPdBi electrocatalyst are 2.133 A $mg_{PtPd}{}^{-1}$ for methanol oxidation reaction and 5.256 A $mg_{PtPd}{}^{-1}$ for ethanol oxidation reaction, which are much better than that of commercial Pt/C and commercial Pd/C. The as-prepared hollow nanocatalyst may be a potential promising electrocatalyst in fuel cells and also may be extended to the applications of other desirable functions.

Keywords: PtPdBi nanocatalyst; hollow structure; electrocatalytic activity; fuel cell

1. Introduction

Fuel cells have a wide range of applications in our daily life because they can transform the chemical energy of fuel to electricity through the electrochemical reaction directly [1,2]. The design of catalysts is part and parcel of fuel cells. Platinum (Pt) and palladium (Pd) are employed as the most effective major catalysts due to their distinct chemical and electronic properties up to present [3,4]. A large number of works associated with Pt-based or Pd-based bimetallic nanocatalysts have been announced, such as PtAg [5], PdRu [6] and so on [7,8]. In the last several years, the synthesis of Pt-based or Pd-based ternary metallic nanostructures has attracted more and more attention. For example, Xu's team has synthesized PdAuNi ternary metallic nanostructure, which is a novel catalyst for application in fuel cells [9]. On the one hand, ternary metallic nanocatalysts can unite the properties of each metal, which leads to exhibiting tri-functional features. On the other hand, ternary metallic nanocatalysts generally reveal properties that differ from monometallic nanocatalysts because the electronic structures of metals can be affected by each other [10,11]. Pd alloyed with Pt may endow metal Pt with the ability to weaken the adsorption of poisoning intermediates, adjust the d-band electronic structure, and enhance the catalytic effect, particularly in catalytically oxidizing towards methanol or ethanol [12–14]. Furthermore, the introduction of bismuth (Bi) can highly enhance the activity in catalysis of Pt or Pd catalysts to methanol oxidation reaction (MOR) or ethanol oxidation reaction (EOR) [15,16]. Pt or Pd combined with Bi can not only accelerate the formation of oxygen-containing species but also facilitate the oxidation of carbonaceous intermediates assimilated on the surface of catalyst, enhancing the specific activity and durability greatly [17–19].

Except alloying with other metals, morphology is a crucial factor influencing the catalytic activity of catalysts greatly. Catalysts with well-controlled morphology are promising materials with improved physical and chemical properties [20]. Plenty of examples can be found in literature with respect to the fascinated structures, including nanoflowers [21], nanowires [22], nanotubes [23], nanosheets [24], nanocubes [25] and hollow-structured nanoparticles [26]. Typically, the hollow structure has been investigated in recent years because of its stability, consecutive reactions and improved selectivity of catalytic reactions [14,27]. In addition, hollow structure provides higher surface area and larger surface to volume ratio, which contributes to enhanced electrocatalytic performance [28,29]. It has been proved that the voids in hollow structures may enrich reagents, leading to increased reaction rates. Pt synchronously alloying with Pd and Bi, along with hollow morphology, may emerge a conjunction effect on MOR and EOR [30]. Nevertheless, few works have been reported about PtPdBi ternary metallic catalysts with hollow structure.

In this work, we described a facile, wet-chemistry synthetic strategy to fabricate ternary metallic hollow PtPdBi nanoparticles at room temperature. The novel ternary metallic hollow PtPdBi nanocatalysts with higher surface area and larger surface to volume ratio can lead to higher electrocatalytic activities toward MOR and EOR. For this reason, the as-prepared hollow PtPdBi nanocatalysts exhibited remarkable catalytic performance in MOR and EOR. The mass activities of as-prepared PtPdBi nanocatalysts are 2.133 A mg $_{PtPd}{}^{-1}$ for MOR and 5.256 A mg $_{PtPd}{}^{-1}$ for EOR, which are much better than the mass activities of commercial Pt/C catalysts and commercial Pd/C catalysts. Moreover, they still exhibit more stable properties than commercial Pt/C and commercial Pd/C, and manifesting such PtPdBi hollow nanocatalysts can be effective and steady catalysts for boosting the development of fuel cells and beyond.

2. Results and Discussion

The hollow PtPdBi nanocatalysts have been synthesized via a facile wet-chemical with the assistance of PVP. The transmission electron microscope (TEM) was first conducted to survey the morphological features and particle size of PtPdBi particles under different magnifications. As shown in Figure 1A,B, PtPdBi ternary metallic particle is composed of a hollow structure with a high yield, indicating that it can be produced at a large scale. The histogram shown in Figure 1C displays that the PtPdBi nanoparticle has a narrow average size distribution and the diameter of the hollow particle ranges from 15.7 nm to 21.4 nm, with the average diameter of 18.4 nm. In addition, this hollow nanoparticle can provide a larger surface areaand leads to the catalyst having the potential to provide higher electrochemical activities. It can be proven that the PtPdBi nanoparticle shows small average diameter and favorable dispersibility, which would be in favor of enhancing the catalytic activity according to the TEM characterization.

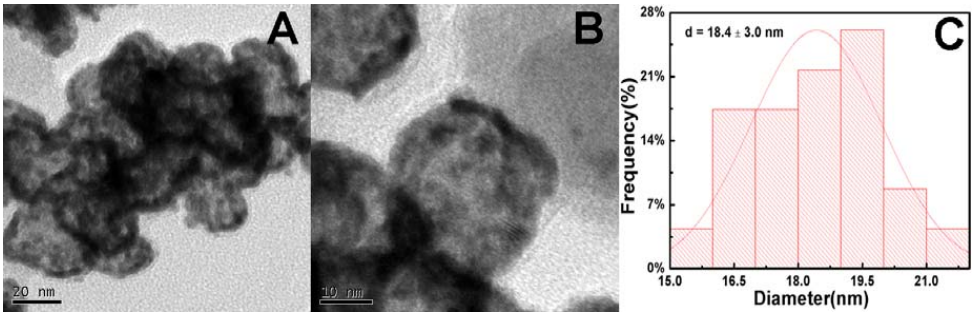

Figure 1. The transmission electron microscope (TEM) (**A**,**B**) images of PtPdBi hollow structure and (**C**) the diameter size distribution of as-prepared PtPdBi particles.

The X-ray diffraction (XRD) experiment was further investigated to determine the crystalline structure of the as-prepared PtPdBi nanoparticles as well as the referenced commercial Pt/C and

commercial Pd/C. As shown in Figure 2, there are two specific diffraction peaks located at around 39.91° and 46.54°, which can be attributed to the face centered cubic (fcc) structure of Pt (JCPDS Card No. 04-0802) or Pd (JCPDS Card No. 87-0641) according to their peak positions and intensities [31,32]. Moreover, the lattice constant of PtPdBi nanoparticles was calculated to be 4.21 Å, while the reported lattice constants of Pt and Pd are 3.92 Å and 3.89 Å. This behavior can be assigned to demonstrate Bi alloyed with Pt and Pd.

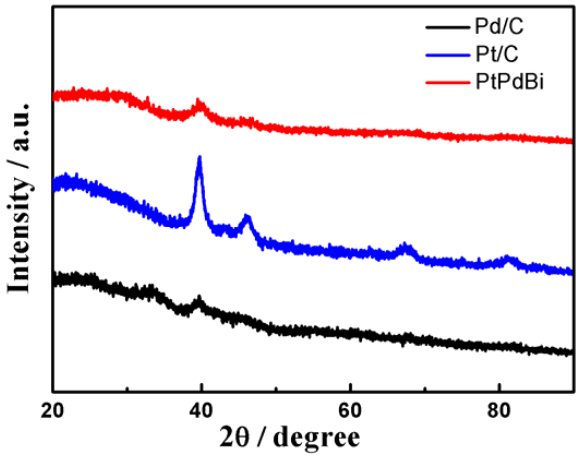

Figure 2. The X-ray diffraction (XRD) patterns of PtPdBi, commercial Pt/C and commercial Pd/C particles.

Fully understanding the surface compositions of the catalysts may be conductive to better studying the properties of electrocatalysts. Therefore, the X-ray photoelectron spectroscopy (XPS) spectra were further utilized to investigate the surface compositions and chemical valence states of Pt, Pd and Bi in the as-prepared hollow PtPdBi nanoparticle. The XPS survey spectra of PtPdBi nanoparticle was shown in Figure 3A, and the appearance of C, N, O can be putted down to the unremoved PVP. Furthermore, it was obvious that Pt, Pd and Bi are found in the spectra. According to the binding energy (BE) data, the chemical state of the surface elements can be analyzed. From the spectra, Pt 4f, Pd 3d and Bi 4f are all separated into metallic state and oxidation state. The Pt 4f peak is indexed into three peaks that can be assigned to Pt (0) and Pt (II), the stronger peaks centered at 71.2 eV ($4f_{7/2}$) and 74.5 eV ($4f_{5/2}$), that can be assigned to the metallic Pt (0) [8]. The weaker peak located at 75.6 eV can be indexed to ionic Pt (II) state. The Pd 3d signals can be fitted into two different species of Pd (0) and Pd (II), one that appeared at 335.4 eV ($3d_{5/2}$) and 340.9 eV ($3d_{3/2}$) is ascribed to metallic Pd (0), while the other weaker one centered at 342.0 eV and 336.5 eV is assigned to the presence of some Pd (II) [33]. In Figure 3D, the peaks of Bi 4f spectrum split into four peaks at 159.2 eV, 159.6 eV, 164.4 eV and 165.0 eV, respectively. The binding energies located at 159.2 eV and 164.4 eV belongs to Bi (0). The doublet at 159.6 eV ($4f_{7/2}$) and 165.0 eV ($4f_{5/2}$) are ascribed to Bi (III) species [34]. Meanwhile, the binding energies of Pt 4f in PtPdBi nanoparticle shift negatively by 0.4 eV at the side of commercial Pt/C, the binding energies of Pd 3d shift positively by 0.4 eV in contrast with commercial Pd/C catalyst, whereas Bi 4f binding energies shift positively by 0.2 eV. The shift of binding energies for Pt, Pd and Bi in PtPdBi nanoparticle can be explained by electronic interactions. Furthermore, the electronic interactions are of significance during the electro-catalytic reaction. Based upon these investigations, we may come to a conclusion that both metallic Pt and Pd are the predominate species in the samples.

After a series of characterizations, the novel morphology, small average diameter and favorable dispersibility of PtPdBi nanoparticles illustrate it will be a splendid catalyst in elextrochemical reactions. In this aspect, the electrocatalytic activity of as-prepared PtPdBi hollow nanocatalyst was assessed through MOR and EOR. Commercial Pt/C and commercial Pd/C were conducted under the same

condition for comparison. Figure 4A displays the cyclic voltammetrys (CVs) on as-prepared PtPdBi nanocatalyst, commercial Pt/C and Pd/C recorded in 1.0 M KOH aqueous solution at a scan rate of 50 mV s^{-1}. The electrochemical active surface area (ECSA) was computed by measuring based on coulombic charge for reducing the oxide of Pt and Pd under the CV curves, assuming that the charge value for the formation of platinum and palladium oxide monolayer is 420 μC cm^{-2}. The ECSAs were figured out to be 21.75 m^2 g^{-1} for PtPdBi nanocatalyst, 14.50 m^2 g^{-1} for commercial Pt/C catalyst and 4.92 m^2 g^{-1} for commercial Pd/C catalyst [35]. The hollow structure endowed the PtPdBi nanocatalyst with higher ECSAs in contrast with that of commercial Pt/C and commercial Pd/C.

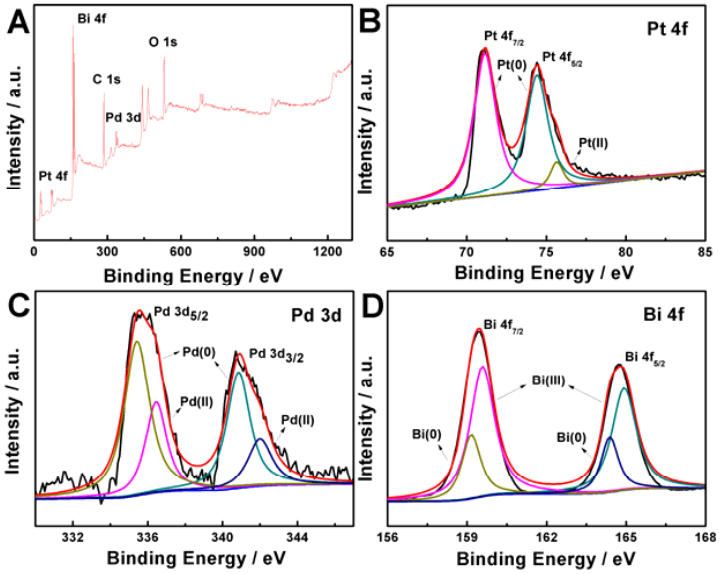

Figure 3. The X-ray photoelectron spectroscopy (XPS) spectra for PtPdBi nanoparticle (**A**); Pt 4f (**B**); Pd 3d (**C**); and Bi 4f (**D**).

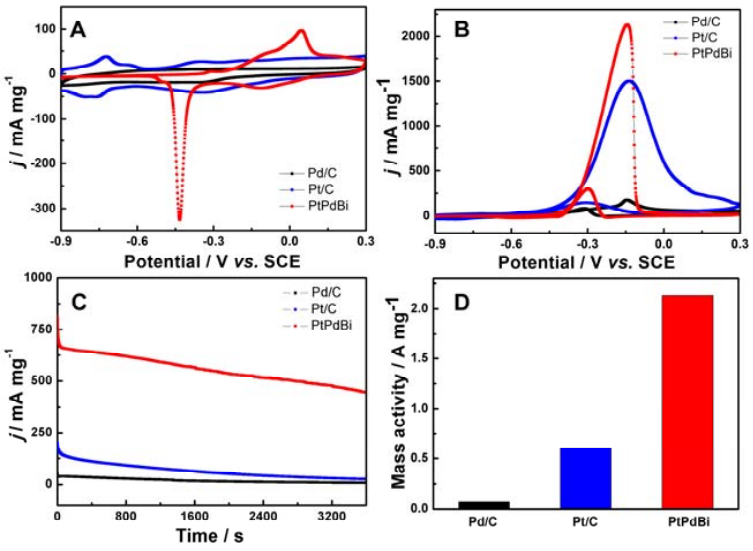

Figure 4. Electrochemistry and electrocatalysis for methanol oxidation reaction (MOR) of PtPdBi nanocatalyst, commercial Pt/C and Pd/C. (**A**) The cyclic voltammetrys CVs of different as-prepared catalysts in 1.0 M KOH aqueous solution at the scan rate of 50 mV s^{-1}; (**B**) CVs of different catalysts in 1.0 M KOH aqueous solution containing 1.0 M CH_3OH solution at the scan rate of 50 mV s^{-1}; (**C**) chronoamperometric curves of different catalysts in 1.0 M KOH aqueous solution containing 1.0 M CH_3OH solution at −0.25 V; (**D**) mass activities of different catalysts calculated from B.

Figure 4B displays the MOR of PtPdBi nanocatalyst, commercial Pt/C and Pd/C catalysts in 1.0 M KOH aqueous solution containing 1.0 M CH_3OH at a scan rate of 50 mV s^{-1}. Under anodic circumstances, each sample has two evident peaks of MOR: the previous current scanning, rising rapidly, is given rise to the typical MOR on the electrode surface, which leads to generating adsorbed carbonaceous intermediates. While the other posterior oxidation scanning is put down to the removal of carbonaceous species, which in the previous scan are not absolutely oxidized. For the sake of comparison, the total mass of Pt and Pd was employed to normalize the current density. The mass activity of PtPdBi nanocatalyst is 2.133 A mg_{PtPd}^{-1}, 3.555-fold enhancements than that of commercial Pt/C (0.600 A mg_{Pt}^{-1}) and 30.471-fold enhancements than that of commercial Pd/C (0.070 A mg_{Pd}^{-1}).

Chronoamperometry experiments in 1.0 M KOH aqueous solution containing 1.0 M CH_3OH at the voltage of −0.25 V to record the electrochemical durability of the catalysts. As shown in Figure 4C, the PtPdBi nanocatalyst reveals slower current decay and maintains the highest limiting currents during the whole period, which clearly demonstrated that the as-synthesized PtPdBi nanocatalyst has good tolerance toward MOR.

To evaluate the electrochemical properties towards EOR, the CVs of these as-obtained nanocatalysts were carried on in 1.0 M KOH aqueous solution containing 1.0 M C_2H_5OH. Similar to the MOR, under anodic circumstances, each sample has two evident peaks of EOR: the previous current scanning, rising rapidly, is given rise to the typical EOR on the electrode surface, which leads to generating adsorbed carbonaceous intermediates. While the other posterior oxidation scanning is put down to the removal of carbonaceous species, which in the previous scan are not absolutely oxidized. The mass activity of PtPdBi nanocatalyst is 5.256 A mg_{PtPd}^{-1}, which is 11.347-fold enhancements and 52.132-fold enhancements than that of commercial Pt/C (0.487 A mg_{Pt}^{-1}) and commercial Pd/C (0.106 A mg_{Pd}^{-1}), respectively. Moreover, after 3600 s, the PtPdBi nanocatalyst remains the highest limiting currents in cronoamperometry experiments, illustrating its excellent durability towards EOR (Figure 5B).

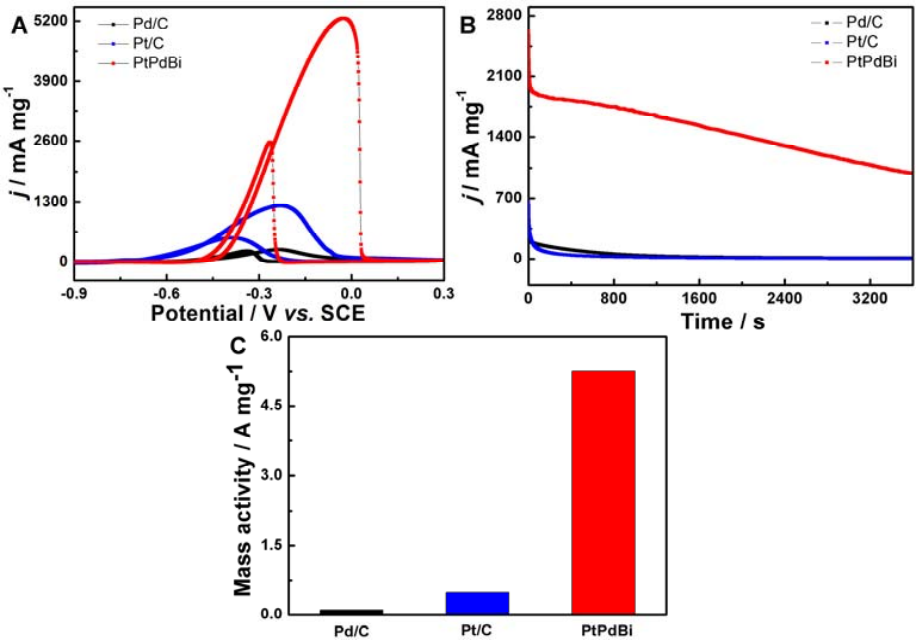

Figure 5. Electrochemistry and electrocatalysis for ethanol oxidation reaction (EOR) of PtPdBi nanocatalyst, commercial Pt/C and commercial Pd/C. (**A**) CVs of different catalysts in 1.0 M KOH aqueous solution containing 1.0 M C_2H_5OH solution at the scan rate of 50 mV s^{-1}; (**B**) chronoamperometric curves of different catalysts in 1.0 M KOH aqueous solution containing 1.0 M C_2H_5OH solution at −0.25 V; (**C**) mass activities of different catalysts calculated from A.

To evaluate the kinetics of electrode reactions and interface processes, as well as the electrochemical characteristics of the as-prepared catalysts, in this work, therefore, we conducted the electrochemical impedance spectroscopy (EIS) for PtPdBi electrocatalysts investigated. The as-prepared PtPdBi nanocatalyst, commercial Pt/C and commercial Pd/C catalyst were tested by EIS at −0.2 V of the as-prepared electrode in 1.0 M KOH aqueous solution containing 1.0 M C_2H_5OH, the equivalent circuit was applied to fit the charge transfer resistances (see Figure 6). In this work, EIS tests are carried out in the frequency ranging from 1 Hz to 100 kHz, while the voltage was kept at a constant potential with a 5 mV voltage perturbation. In general, the charge-transfer resistance of the catalyst is in direct proportion to the diameter of the semicircle, and the smaller diameter of the impedance arc (DIA), the minor charge-transfer resistance for EOR will be. The figure visually reveals that the DIAs of the PtPdBi, commercial Pt/C and commercial Pd/C catalysts showed the order as follows: PtPdBi < Pt/C < Pd/C, indicating that the as-obtained PtPdBi nanocataltsts possess the apparently small electron transfer resistance (R_{ct}) than that of commercial Pt/C and commercial Pd/C. The smallest DIA on PtPdBi means that the PtPdBi hollow nanocatalyst has higher charge transport performances and better electrocatalytic activity for EOR than the other electrodes. For the equivalent circuit, R_s represents the solution resistance, and R_{ct} represents the charge-transfer resistance for the process of ethanol electrocatalytic oxidation. Overall, the R_{ct} on PtPdBi is much smaller than those on commercial Pt/C and Pd/C catalysts, indicating the electron transfer for ethanol oxidation on PtPdBi is much easier, which could enhance the electrocatalytic activity of the catalyst for ethanol oxidation [36]. Hence, the consequence of EIS further confirmed the augment in electrocatalytic activity of the PtPdBi catalyst.

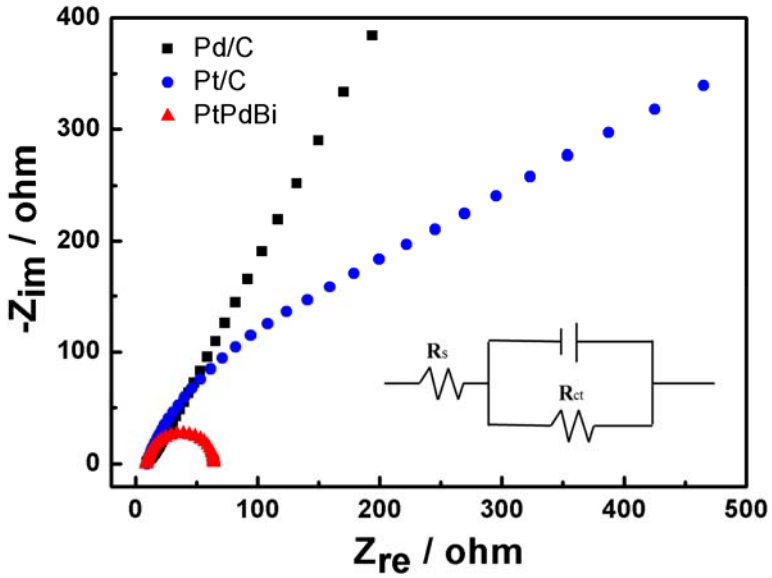

Figure 6. Nyquist plots of ethanol electrooxidation on the PtPdBi nanocatalyst, commercial Pt/C and commercial Pd/C electrodes in 1.0 M KOH aqueous solution containing 1.0 M C_2H_5OH solution at the voltage of −0.2 V. The insert was the equivalent circuit used to fit the impedance spectra.

3. Materials and Methods

3.1. Chemicals

Palladium (II) chloride ($PdCl_2$), hexachloroplatinic (IV) acid hexahydrate ($H_2PtCl_6 \cdot 6H_2O$), bismuth (III) nitrate pentahydrate ($Bi(NO_3)_3 \cdot 5H_2O$), sodium borohydride ($NaBH_4$, 96.0%) and ethanol (C_2H_5OH) were purchased from Sinopharm Chemical Reagent Co. Ltd. (Shanghai, China); commercial Pd/C (JM 20% Pd) and commercial Pt/C (JM 20% Pt) were bought in Shanghai Hesen Electric Co., Ltd. (Shanghai, China); polyvinylpyrrolidone (PVP, K30) was purchased in Shanghai Lingfeng Chemical

Reagent Co., Ltd. (Shanghai, China). During this work, all of the chemicals were employed under analytical grade, and the needed water used during the whole work was double-distilled (DI) water.

3.2. Preparation of PtPdBi NPs

In a typical synthesis of PtPdBi nanoparticles, 100 mg PVP, 5.5 mg $Bi(NO_3)_3 \cdot 5H_2O$, 60 mg $NaBH_4$ and 10 mL DI water were added into a 25 mL glass vial, which is fixed on a magnetic stirrer. Then, 0.5 mL of 22.56 mM H_2PdCl_4 solution (solution 1) was followed and added under vigorous stirring. Then, half an hour passed before 1.46 mL H_2PtCl_6 (solution 2) was dropwise injected into the above solution. The reaction solution was continuously stirred for 4 h at room temperature. The achieved mixture was sent to centrifuge and washed a few times with DI water, acetone and ethanol. Furthermore, 22.56 mM H_2PdCl_4 solution (solution 1) was prepared by adding 1 g $PdCl_2$ into 0.94 mL HCl and then diluted to 250 mL with DI water. Finally, 7.723 mM H_2PtCl_6 solution (solution 2) was prepared by dissolving 1 g H_2PtCl_6 into DI water and then diluted to 250 mL.

3.3. Characterizations

For characterizing the physicochemical properties of the as-obtained products, a series of analyses have been employed. The morphology and structure of the samples were characterized on a TECNAI-G20 transmission electron microscope (TEM) (FEI, Hong Kong, China) at an accelerating voltage of 200 kV. X-ray diffraction (XRD) analysis operated on a PANalytical X'Pert Pro MRD system (PANalytical, Amsterdam, The Netherlands) at 40 kV and the current at 30 mA with Cu Kα radiation source (λ = 1.54056 Å) at a step scan of 20° min^{-1} from 5° to 90° was also measured to investigate microcrystal structure properties. In addition, the X-ray photoelectron spectroscopy (XPS) was performed on a VG Scientific ESCALab 220XL electron spectrometer (Thermo Fisher Scientific, Waltham, MA, USA), using 300 W Al Kα radiation, was also employed to study the element valences and compositions of different samples.

3.4. Electrochemical Measurements

All of the electrochemical measurements of all the as-prepared samples were carried out at room temperature with a CHI 760 E electrochemical workstation purchased from Shanghai CH Instrumental Co., (Shanghai, China). A typical three-electrode test cell was put to test the electrochemical measurements. A platinum wire and a saturated calomel electrode (SCE) were applied to serve as reference electrode and counter electrode, respectively. In this work, we used the glassy carbon electrode (GCE, diameter of 3.0 mm, area: 7 mm^2) as working electrode, which needs to be polished with alumina powders until an apinoid surface was obtained every time before examination. The polished GCE was then rinsed through ultrasonication in DI water and ethanol for 30 s probably. To achieve the catalyst-coated working electrode, the as-prepared PtPdBi catalyst was decentralized in 10 mL DI water to form a 0.34 mg_{PtPd}/mL suspension, and then the ultrasound was dispersed evenly. Furthermore, 10 μL of the as-prepared catalyst suspension was loaded on the GCE surface using a micropipette and then dried in a drying oven. The calculation of integration of the hydrogen adsorption charge under the cyclic voltammetry (CV) in 1.0 M KOH aqueous solution at room temperature is defined as electrochemical active surface area (ECSA) in this work. The CV measurements were conducted in the potential window between −0.9 and 0.3 V with the scan rate of 50 mV s^{-1}. MOR was conducted in a 1.0 M KOH aqueous solution containing 1.0 M CH_3OH. EOR was conducted in a 1.0 M KOH containing 1.0 M C_2H_5OH. The sweep speed of both of MOR and EOR was 50 mV s^{-1} (−0.9~0.3 V). For the sake of comparison, commercial Pd/C and commercial Pt/C were used as contrastive catalysts, and the uniform processes as mentioned above were applied to perform the electrochemical measurements.

4. Conclusions

In conclusion, we have demonstrated a wet-chemical, facile synthetic method of hollow PtPdBi ternary metallic electrocatalyst. The as-prepared PtPdBi electrocatalyst revealed enhanced electrocatalytic activity towards MOR and EOR, which may be ascribed to the synergistic effect between Pt, Pd and Bi. The mass activity of PtPdBi electrocatalyst is 2.133 A $mg_{PtPd}{}^{-1}$ for MOR and 5.256 A $mg_{PtPd}{}^{-1}$ for EOR, which is much higher than that of commercial Pt/C and commercial Pd/C catalysts. These demonstrate that PtPdBi hollow nanomaterial is a promising progressive electrocatalyst for fuel cells with its splendid activity and durability.

Acknowledgments: This work was supported by the National Natural Science Foundation of China (Grant No. 51373111), the Suzhou Industry (SYG201636), the Priority Academic Program Development of Jiangsu Higher Education Institutions (PAPD) and the State and Loc-al Joint Engineering Laboratory for Novel Functional Polymeric Materials.

Author Contributions: Zhiping Xiong and Yukou Du conceived and designed the experiments; Zhiping Xiong performed the experiments; Shumin Li and Bo Yan analyzed the data; Hui Xu and Ke Zhang contributed reagents/materials/analysis tools; and Zhiping Xiong wrote the paper.

Conflicts of Interest: The authors declare no conflict of interest. The founding sponsors had no role in the design of the study; in the collection, analyses, or interpretation of data; in the writing of the manuscript, and in the decision to publish the results.

References

1. Zhang, N.; Guo, S.; Zhu, X.; Guo, J.; Huang, X. Hierarchical Pt/Pt_xPb core/shell nanowires as efficient catalysts for electrooxidation of liquid fuels. *Chem. Mater.* **2016**, *28*, 4447–4452. [CrossRef]
2. Strasser, P.; Koh, S.; Anniyev, T.; Greeley, J.; More, K.; Yu, C.; Liu, Z.; Kaya, S.; Nordlund, D.; Ogasawara, H.; et al. Lattice-strain control of the activity in dealloyed core-shell fuel cell catalysts. *Nat. Chem.* **2010**, *2*, 454–460. [CrossRef] [PubMed]
3. Li, F.-M.; Gao, X.-Q.; Li, S.-N.; Chen, Y.; Lee, J.-M. Thermal decomposition synthesis of functionalized PdPt alloy nanodendrites with high selectivity for oxygen reduction reaction. *NPG Asia Mater.* **2015**, *7*, e219. [CrossRef]
4. Hong, J.W.; Kang, S.W.; Choi, B.S.; Kim, D.; Lee, S.B.; Han, S.W. Controlled synthesis of Pd-Pt alloy hollow nanostructures with enhanced catalytic activities for oxygen reduction. *ACS Nano* **2012**, *6*, 2410–2419. [CrossRef] [PubMed]
5. Wang, C.; Yue, R.; Wang, H.; Zou, C.; Du, J.; Jiang, F.; Du, Y.; Yang, P.; Wang, C. Dendritic Ag@Pt core-shell catalyst modified with reduced graphene oxide and titanium dioxide: Fabrication, characterization, and its photo-electrocatalytic performance. *Int. J. Hydrogen Energy* **2014**, *39*, 5764–5771. [CrossRef]
6. Lim, E.J.; Kim, Y.; Choi, S.M.; Lee, S.; Noh, Y.; Kim, W.B. Binary PdM catalysts (M = Ru, Sn, or Ir) over a reduced graphene oxide support for electro-oxidation of primary alcohols (methanol, ethanol, 1-propanol) under alkaline conditions. *J. Mater. Chem. A* **2015**, *3*, 5491–5500. [CrossRef]
7. Mao, J.; Liu, Y.; Chen, Z.; Wang, D.; Li, Y. Bimetallic Pd-Cu nanocrystals and their tunable catalytic properties. *Chem. Commun.* **2014**, *50*, 4588–4591. [CrossRef] [PubMed]
8. Liu, X.-Y.; Zhang, Y.; Gong, M.-X.; Tang, Y.-W.; Lu, T.-H.; Chen, Y.; Lee, J.-M. Facile synthesis of corallite-like Pt–Pd alloy nanostructures and their enhanced catalytic activity and stability for ethanol oxidation. *J. Mater. Chem. A* **2014**, *2*, 13840. [CrossRef]
9. Li, S.; Lai, J.; Luque, R.; Xu, G. Designed multimetallic Pd nanosponges with enhanced electrocatalytic activity for ethylene glycol and glycerol oxidation. *Energy Environ. Sci.* **2016**, *9*, 3097–3102. [CrossRef]
10. Mao, J.; Cao, T.; Chen, Y.; Wu, Y.; Chen, C.; Peng, Q.; Wang, D.; Li, Y. Seed-mediated synthesis of hexameric octahedral PtPdCu nanocrystals with high electrocatalytic performance. *Chem. Commun.* **2015**, *51*, 15406–15409. [CrossRef] [PubMed]
11. Li, S.-J.; Ping, Y.; Yan, J.-M.; Wang, H.-L.; Wu, M.; Jiang, Q. Facile synthesis of AgAuPd/graphene with high performance for hydrogen generation from formic acid. *J. Mater. Chem. A* **2015**, *3*, 14535–14538. [CrossRef]
12. Saleem, F.; Ni, B.; Yong, Y.; Gu, L.; Wang, X. Ultra-small tetrametallic Pt-Pd-Rh-Ag nanoframes with tunable behavior for direct formic acid/methanol oxidation. *Small* **2016**, *12*, 5261–5268. [CrossRef] [PubMed]

13. Lu, Y.; Jiang, Y.; Wu, H.; Chen, W. Nano-PtPd cubes on graphene exhibit enhanced activity and durability in methanol electrooxidation after CO stripping-cleaning. *J. Phys. Chem. C* **2013**, *117*, 2926–2938. [CrossRef]
14. Liu, B.; Li, H.Y.; Die, L.; Zhang, X.H.; Fan, Z.; Chen, J.H. Carbon nanotubes supported PtPd hollow nanospheres for formic acid electrooxidation. *J. Power Sources* **2009**, *186*, 62–66. [CrossRef]
15. Xu, H.; Yan, B.; Zhang, K.; Wang, C.; Zhong, J.; Li, S.; Yang, P.; Du, Y. Facile synthesis of Pd-Ru-P ternary nanoparticle networks with enhanced electrocatalytic performance for methanol oxidation. *Int. J. Hydrogen Energy* **2017**, *42*, 11229–11238. [CrossRef]
16. Gu, Z.; Bin, D.; Feng, Y.; Zhang, K.; Wang, J.; Yan, B.; Li, S.; Xiong, Z.; Wang, C.; Shiraishi, Y.; et al. Seed-mediated synthesis of cross-linked Pt-NiO nanochains for methanol oxidation. *Appl. Surf. Sci.* **2017**, *411*, 379–385. [CrossRef]
17. Liao, H.; Zhu, J.; Hou, Y. Synthesis and electrocatalytic properties of PtBi nanoplatelets and PdBi nanowires. *Nanoscale* **2014**, *6*, 1049–1055. [CrossRef] [PubMed]
18. Neto, A.O.; Tusi, M.M.; de Oliveira Polanco, N.S.; da Silva, S.G.; Coelho dos Santos, M.; Spinacé, E.V. PdBi/C electrocatalysts for ethanol electro-oxidation in alkaline medium. *Int. J. Hydrogen Energy* **2011**, *36*, 10522–10526. [CrossRef]
19. Ji, X.; Lee, K.T.; Holden, R.; Zhang, L.; Zhang, J.; Botton, G.A.; Couillard, M.; Nazar, L.F. Nanocrystalline intermetallics on mesoporous carbon for direct formic acid fuel cell anodes. *Nat. Chem.* **2010**, *2*, 286–293. [CrossRef] [PubMed]
20. Li, C.; Sato, T.; Yamauchi, Y. Electrochemical synthesis of one-dimensional mesoporous Pt nanorods using the assembly of surfactant micelles in confined space. *Angew. Chem.* **2013**, *52*, 8050–8053. [CrossRef] [PubMed]
21. Bin, D.; Yang, B.; Zhang, K.; Wang, C.; Wang, J.; Zhong, J.; Feng, Y.; Guo, J.; Du, Y. Design of PdAg hollow nanoflowers through galvanic replacement and their application for ethanol electrooxidation. *Chem. Eur. J.* **2016**, *22*, 16642–16647. [CrossRef] [PubMed]
22. Keng, P.Y.; Kim, B.Y.; Shim, I.B.; Sahoo, R.; Veneman, P.E.; Armstrong, N.R.; Yoo, H.; Pemberton, J.E.; Bull, M.M.; Griebel, J.J.; et al. Colloidal polymerization of polymer-coated ferromagnetic nanoparticles into cobalt oxide nanowires. *ACS Nano* **2009**, *3*, 3143–3157. [CrossRef] [PubMed]
23. Shi, X.; Han, S.; Sanedrin, R.J.; Galvez, C.; Ho, D.G.; Hernandez, B.; Zhou, F.; Selke, M. Formation of cobalt oxide nanotubes: Effect of intermolecular hydrogen bonding between Co(III) complex precursors incorporated onto colloidal templates. *Nano Lett.* **2002**, *2*, 289–293. [CrossRef]
24. Yoo, E.; Okata, T.; Akita, T.; Kohyama, M.; Makamura, J.; Honma, I. Enhanced electrocatalytic activity of Pt subnanoclusters on graphene nanosheet surface. *Nano Lett.* **2009**, *9*, 2255–2259. [CrossRef] [PubMed]
25. Wang, C.; Daimon, H.; Lee, Y.; Kim, J.; Sun, S. Synthesis of monodisperse Pt nanocubes and their enhanced catalysis for oxygen reduction. *J. Am. Chem. Soc.* **2007**, *129*, 6974–6975. [CrossRef] [PubMed]
26. Wang, D.; Yu, Y.; He, H.; Wang, J.; Zhou, W.; Abruna, H.D. Template-free synthesis of hollow structured Co3O4 nanoparticles as high-performance anodes for lithium-ion batteries. *ACS Nano* **2015**, *9*, 1775–1781. [CrossRef] [PubMed]
27. Prieto, G.; Tuysuz, H.; Duyckaerts, N.; Knossalla, J.; Wang, G.H.; Schuth, F. Hollow nano- and microstructures as catalysts. *Chem. Rev.* **2016**, *116*, 14056–14119. [CrossRef] [PubMed]
28. Yang, S.; Wang, C.; Chen, L.; Chen, S. Facile dicyandiamide-mediated fabrication of well-defined CuO hollow microspheres and their catalytic application. *Mater. Chem. Phys.* **2010**, *120*, 296–301. [CrossRef]
29. Da Silva, A.G.M.; Rodrigues, T.S.; Taguchi, L.S.K.; Fajardo, H.V.; Balzer, R.; Probst, L.F.D.; Camargo, P.H.C. Pd-based nanoflowers catalysts: Controlling size, composition, and structures for the 4-nitrophenol reduction and BTX oxidation reactions. *J. Mater. Sci.* **2015**, *51*, 603–614. [CrossRef]
30. Huang, L.; Han, Y.; Dong, S. Highly-branched mesoporous Au-Pd-Pt trimetallic nanoflowers blooming on reduced graphene oxide as an oxygen reduction electrocatalyst. *Chem. Commun.* **2016**, *52*, 8659–8662. [CrossRef] [PubMed]
31. Eid, K.; Wang, H.; Malgras, V.; Alothman, Z.A.; Yamauchi, Y.; Wang, L. Trimetallic PtPdRu dendritic nanocages with three-dimensional electrocatalytic surfaces. *J. Phys. Chem. C* **2015**, *119*, 19947–19953. [CrossRef]
32. Li, T.; Huang, Y.; Ding, K.; Wu, P.; Abbas, S.C.; Ghausi, M.A.; Zhang, T.; Wang, Y. Newly designed PdRuBi/N-Graphene catalysts with synergistic effects for enhanced ethylene glycol electro-oxidation. *Electrochim. Acta* **2016**, *191*, 940–945. [CrossRef]

33. Guo, Y.; Xu, Y.-T.; Zhao, B.; Wang, T.; Zhang, K.; Yuen, M.M.F.; Fu, X.-Z.; Sun, R.; Wong, C.-P. Urchin-like Pd@CuO–Pd yolk–shell nanostructures: Synthesis, characterization and electrocatalysis. *J. Mater. Chem. A* **2015**, *3*, 13653–13661. [CrossRef]
34. Xu, H.; Zhang, K.; Yan, B.; Wang, J.; Wang, C.; Li, S.; Gu, Z.; Du, Y.; Yang, P. Ultra-uniform PdBi nanodots with high activity towards formic acid oxidation. *J. Power Sources* **2017**, *356*, 27–35. [CrossRef]
35. Łukaszewski, M. Electrochemical methods of real surface area determination of noble metal electrodes—An overview. *Int. J. Electrochem. Sci.* **2016**, *11*, 4442–4469. [CrossRef]
36. Ren, F.; Zhai, C.; Zhu, M.; Wang, C.; Wang, H.; Bin, D.; Guo, J.; Yang, P.; Du, Y. Facile synthesis of PtAu nanoparticles supported on polydopamine reduced and modified graphene oxide as a highly active catalyst for methanol oxidation. *Electrochim. Acta* **2015**, *153*, 175–183. [CrossRef]